Utilizing CryoSat-2 sea ice thickness to initialize a coupled ice-ocean modeling system

Richard A. Allard [a,*], Sinead L. Farrell [b], David A. Hebert [a], William F. Johnston [c], Li Li [d], Nathan T. Kurtz [e], Michael W. Phelps [f], Pamela G. Posey [a], Rachel Tilling [g], Andy Ridout [h], Alan J. Wallcraft [i]

[a] *Naval Research Laboratory, Oceanography Division, 1009 Balch Blvd, Stennis Space Center, MS 39529, USA*
[b] *Earth System Science Interdisciplinary Center (ESSIC), University of Maryland, 5830 University Research Ct., College Park, MD 20740, USA*
[c] *Computational Physics, Inc., 2750 Prosperity Ave Suite 600, Fairfax, VA 22031, USA*
[d] *Naval Research Laboratory, Remote Sensing Division, 4555 Overlook Ave, Washington, DC 20375, USA*
[e] *NASA Goddard Space Flight Center, Cryospheric Sciences Laboratory, Greenbelt, MD 20771, USA*
[f] *Jacobs Technology Inc., 1009 Balch Blvd, Stennis Space Center, MS 39529, USA*
[g] *Center for Polar Observations and Modelling, School of Earth and Environment, University of Leeds, Leeds LS29JT, UK*
[h] *Center for Polar Observations and Modelling, Earth Sciences Department, University College London, London WC1E6BT, UK*
[i] *Center for Ocean-Atmospheric Prediction Studies (COAPS), Florida State University, Tallahassee, FL 32310, USA*

Abstract

Two CryoSat-2 sea ice thickness products derived with independent algorithms are used to initialize a coupled ice-ocean modeling system in which a series of reanalysis studies are performed for the period of March 15, 2014–September 30, 2015. Comparisons against moored upward looking sonar, drifting ice mass balance buoy, and NASA Operation IceBridge ice thickness data show that the modeling system exhibits greatly reduced bias using the satellite-derived ice thickness data versus the operational model run without these data. The model initialized with CryoSat-2 ice thickness exhibits skill in simulating ice thickness from the initial period to up to 6 months. We find that the largest improvements in ice thickness occur over multi-year ice. Based on the data periods examined here, we find that for the 18-month study period, when compared with upward looking sonar measurements, the CryoSat-2 reanalyses show significant improvement in bias (0.47–0.75) and RMSE (0.89–1.04) versus the control run without these data (1.44 and 1.60, respectively). An ice drift comparison reveals little change in ice velocity statistics for the Pan Arctic region; however some improvement is seen during the summer/autumn months in 2014 for the Bering/Beaufort/Chukchi and Greenland/Norwegian Seas. These promising results suggest that such a technique should be used to reinitialize operational sea ice modeling systems.

1. Introduction

Arctic sea ice extent has been on the decline for the past several decades (Parkinson and Cavalieri, 2008). The March and September Northern Hemisphere sea ice extent has declined on average 2.7% and 13.3% per decade, respectively, for the period of 1979–2016 (Perovich et al., 2016). Multi-year ice (MYI) has been in decline for the past 3 decades, with ice older than 4 years accounting for 20% of the total ice composition in the mid-1980s compared to only a few percent since 2012 (Perovich et al., 2016;

Tschudi et al., 2016). Also, first-year ice (FYI) has accounted for 60–70% of the March ice pack since 2008. Markus et al. (2009) investigated passive microwave satellite data for the period of 1979–2008 and found the average length of the melt season had increased by 6.4 days per decade over the 30-year period for the entire Arctic, with the Chukchi/Beaufort and Laptev/East Siberian Seas showing trends of 12.0 and 11.3 days per decade, respectively.

The observed changes in Arctic sea ice provide motivation to assess and improve sea ice forecasting capabilities. The following three paragraphs describe ice thickness measurements obtained from European Remote Sensing (ERS-1 and -2) platforms, Ice, Cloud, and land Elevation Satellite (ICESat), CryoSat-2 and NASA Operation IceBridge (OIB). An overview of seasonal forecasting since 2008 follows, with the remaining paragraphs describing models and modeling systems and how they have been used to measure the decline in sea ice extent and volume. We also include a paragraph describing the importance of snow depth on ice thickness retrievals.

Measurements from radar altimeters on the ERS-1 and ERS-2 platforms provided the first basin-scale mappings of Arctic sea ice thickness for the period 1993–2001 (Laxon et al., 2003), although to a latitudinal limit of 81.5°N. Laser altimeter data from ICESat extended the observations to nearly Arctic-wide coverage, and provided seasonal (autumn and winter) ice thickness mappings from 2003 to 2008 (Kwok et al., 2007, 2009). Kwok and Rothrock (2009) examined submarine data for the period of 1958–2008 and available ICESat data and found a significant decline in mean winter ice thickness from 3.64 m in 1980 to 1.89 m in 2008. Haas et al. (2008) collected helicopter-borne electromagnetic measurements of ice thickness in the Transpolar Drift for the years 2001, 2004 and 2007, and found a 44% reduction in mean ice thickness since 2001.

CryoSat-2 (Laxon et al., 2013; Kurtz et al., 2014), launched in April 2010, provides surface elevation, which can be converted to ice freeboard, during the months of January–May and October–December of each year. CryoSat-2 (CS2) data is not available during summer months due to signal contamination resulting from snow/ice melt, open water and melt ponds.

NASA OIB (Kurtz et al., 2013; Richter-Menge and Farrell, 2013) initiated the collection of Arctic ice thickness and snow depth measurements from airborne platforms in March/April 2009 to bridge the gap in satellite-borne measurements of ice freeboard between ICESat and the planned 2018 launch of ICESat-2. Antarctic OIB surveys were also initiated in 2009 and are conducted in the October/November time frame. This paper focuses on the assimilation of Arctic data. OIB provides freeboard estimates derived from an airborne LIDAR which when combined with snow depth estimates from an ultra-wideband snow radar are converted to ice thickness (Farrell et al., 2012; Kurtz et al., 2013, 2014). The OIB surveys were designed to complement the satellite-based estimates of

ice thickness from CS2 and helicopter- and aircraft-mounted electro-magnetic (EM) measurements (Haas et al., 2008, 2010) of ice thickness. For example, a comparison of OIB sea ice thickness data collected during the March-April 2014 survey with CS2 thickness estimates (Laxon et al., 2013) for the same period is shown in Fig. 1. There is excellent agreement (mean difference of 0.15 m, and correlation coefficient of 0.71) between the two independent measures of Arctic ice thickness, with both clearly showing a gradient from thicker, older ice north of Greenland and the Canadian Arctic Archipelago, to thinner ice in the FYI regions of the Beaufort, Chukchi, East Siberian, Laptev, Kara and Barents Seas. Richter-Menge and Farrell (2013) examined OIB data in the western Arctic Ocean for the period of March/April 2009–2013. They found that the central Arctic was dominated by MYI with a mean thickness of 3.2 m, while the southern Beaufort and Chukchi Sea region containing a mixture of 75% FYI and 25% MYI, and found mean thicknesses decreased from near 2.5 m to a low of 1.6 m during the five-year period.

The importance of sea ice thickness for seasonal and longer-term forecasts of sea ice extent has been investigated by several researchers. Lindsay et al. (2008) utilized the Pan-Arctic Ice-Ocean Modeling and Assimilation System (PIOMAS) to study seasonal predictions of sea ice extent. They found that the pan-Arctic forecast skill relative to climatology was 0.77 with a six month lead time for a forecast initialized in March. They determined that ice concentration was the dominant factor in the first 2 months and the ocean temperature of the model layer with a depth between 200 and 270 m was most important for longer lead times. Holland et al. (2011) used the Community Climate System Model version 3 to study the predictability of the summer sea ice extent. They found that winter preconditioning provides some summer ice area predictability and stressed the importance of feedback to the atmosphere. Day et al. (2014) performed experiments with the Hadley Centre Global Environmental Model version 1.2 (HadGEM1.2) coupled atmosphere-ocean-ice modeling system. Twin experiments revealed that initializing the sea ice model on July 1 showed improved skill in predicting the September sea ice extent compared to a control climatological initialization. Blanchard-Wrigglesworth and Bitz (2014) studied fully coupled General Circulation Models (GCMs) and sea ice-ocean models that were forced with observation estimates derived from atmospheric reanalysis and satellite measurements. They found that sea ice thickness anomalies have a typical time scale of approximately 6–20 months with a typical length scale of 500–1000 km. They hypothesized that the number of ice monitoring locations needed to characterize the full Arctic basin sea ice thickness is model dependent and the variability would vary between 3 and 14 locations. Guemas et al. (2016) presented a review of Arctic sea-ice prediction on seasonal to decadal time-scales. Using dynamical and ensemble-based forecasting systems designed to run on decadal time-
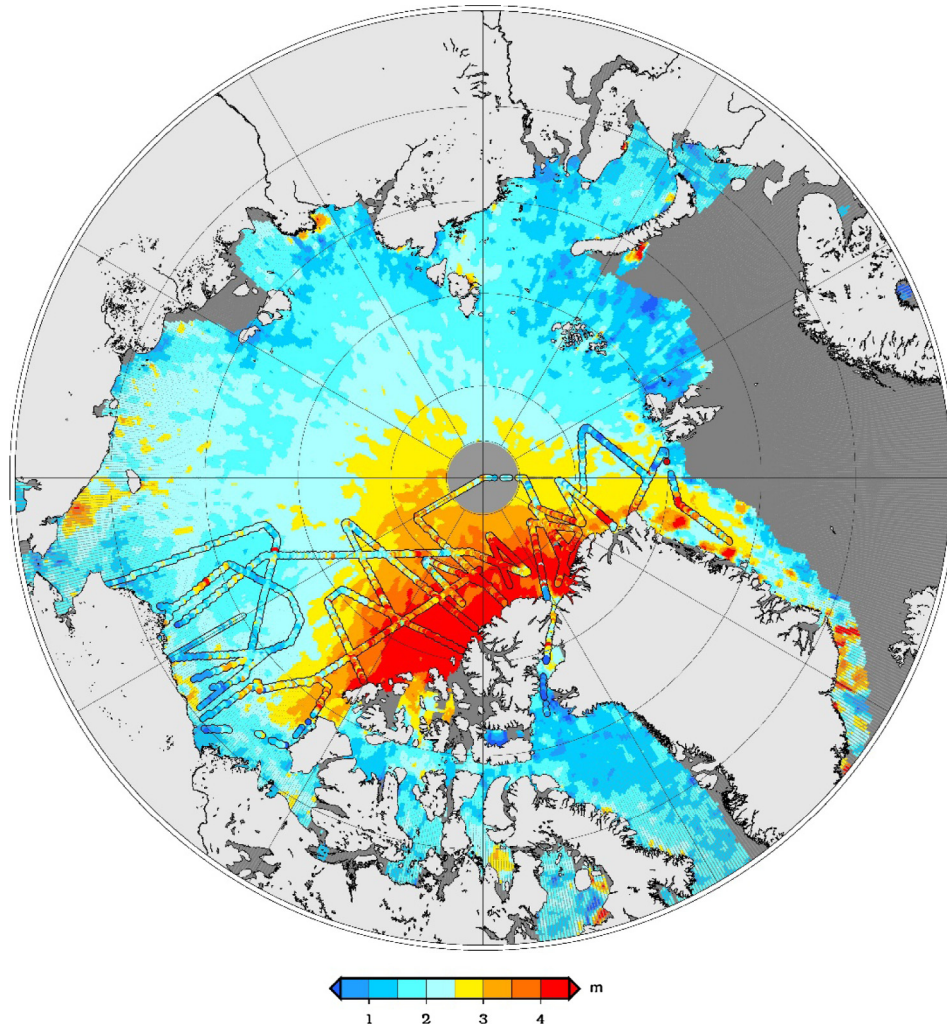
Fig. 1. Map of OIB (quicklook) sea ice thickness data collected during March & April 2014 overlaid on the CS2-CPOM thickness data for the period 1 March 2014–30 April 2014.

scales, they concluded that predictability mainly originates from persistence or advection of sea-ice anomalies, interactions with ocean and atmosphere, and changes in radiative forcing.

Schweiger et al. (2011) performed an uncertainty analysis with PIOMAS to examine changes in Arctic ice volume using a host of observations and satellite-derived data for the period of 1979–2010. Using this approach, they estimated a "conservative" value of -2.8×10^3 km^3/decade. Laxon et al. (2013) estimated changes in Arctic ice volume for the 2003–2008 ICESat period and the winters of 2010/2011 and 2011/2012 using CS2 data and found a significant decline of 4291 km^3 for autumn and 1479 km^3 in winter ice volume during the period. Tilling et al. (2015) used CS2 measurements for the period of 2011–2015 to study changes in Arctic sea ice volume and found a 14% reduction in autumn ice volume between 2010 and 2012, but an increase of 33% and 25% respectively, for 2013 and 2014. They attributed the volume increase to the retention of thick sea ice northwest of Greenland and an associated 5% reduction in the number of melting days.

Numerous studies have examined the impact of snow depth on ice thickness retrievals. Giles et al. (2007) found that the largest component of the error in retrieved ice thickness was due to uncertainties in snow depth. Ricker et al. (2015) examined ice and snow freeboard measurements from Arctic Ice Mass Balance Buoys (IMBB) and coincident CS2 measurements from 2012 to 2014 and determined that snowfall had a significant impact on CS2 retrievals of ice freeboard. Webster et al. (2014) evaluated the spring snow depth distribution from airborne OIB observations during 2009–2013 and found a snow depth loss of 12.8 cm (37%) in the western Arctic and 18.3 cm (56%) in the Chukchi and Beaufort seas compared to snow observations from 1937 and 1954–1991 Soviet drifting ice stations (Warren et al., 1999). King et al. (2015) examined OIB quick-look snow depth estimates and found reasonable agreement with *in situ* observations on level ice, but deformed FYI and MYI and surface roughness contributed to higher uncertainties in the retrieved snow, which are ultimately propagated to uncertainties in ice thickness in the OIB product. Remaining uncertainties
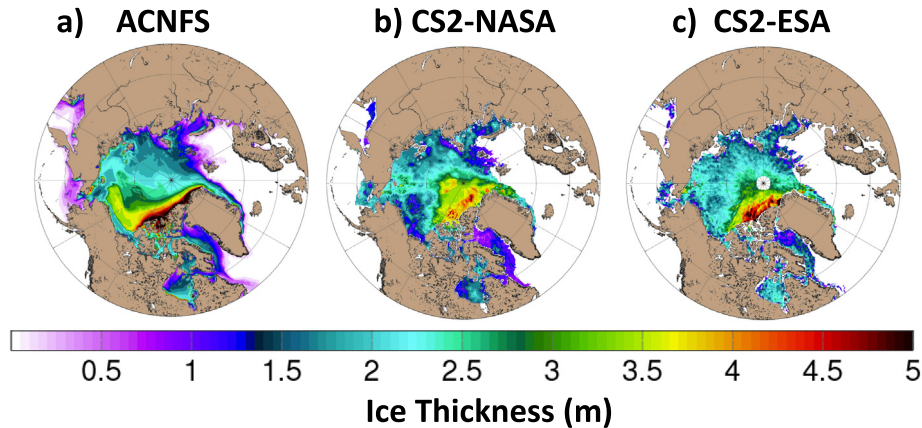
Fig. 2. Monthly averaged March 2014 sea ice thickness (m) for (a) operational ACNFS (b) CS2-NASA, and (c) CS2-CPOM.
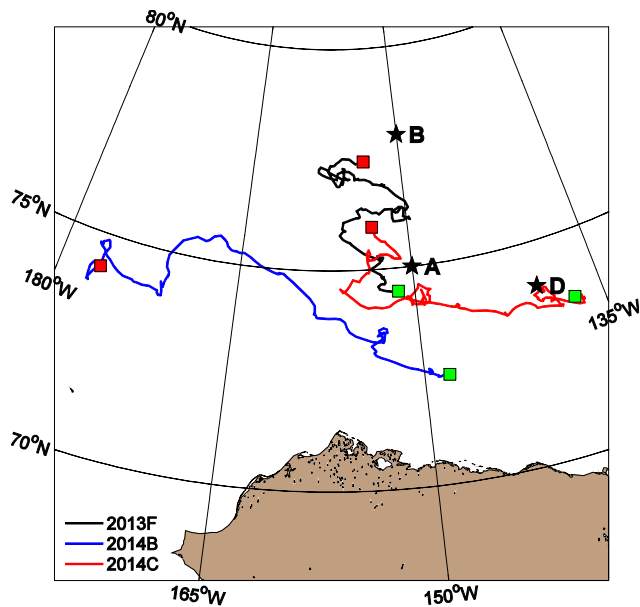

Fig. 3. Location of ULS moorings (black stars) labeled as "A", "B", and "D". CRREL Ice Mass Balance buoys (colored lines) (Perovich et al., 2017) for 2013F (black), 2014B (blue) and 2014C (red). Green and red squares denote the start and end locations for the buoys. (For interpretation of the references to colour in this figure legend, the reader is referred to the web version of this article.)

associated with the assumptions for the densities of ice and snow, used to convert freeboard measurements to thickness, also contribute to small uncertainties in the derived ice thickness products (Giles et al., 2007).

Johnson et al. (2012) examined forecast skill of modeled monthly ice thickness in 6 ice modeling systems as part of the Arctic Ocean Model Intercomparison Project utilizing gridded ice thickness from ICESat (2004–2008), EM (2001–2009), ice draft data from 24 upward looking sonar (ULS) moorings in the Beaufort Sea, Fram Strait and Greenland Sea, *in situ* drill hole, and submarine data from 1975 to 2000. Each modeling system used different forcing, boundary conditions, and numerical methods. They found that the models, on average, overestimated the thickness of

ice thinner than 2 m, and underestimated the thickness of ice thicker greater than 2 m. Collow et al. (2015) found an improved sea ice seasonal cycle when their coupled modeling system was initialized with ice thickness from the PIOMAS model (Schweiger et al., 2011) which assimilated ice concentration and sea surface temperature, but not actual ice thickness data.

Lisæter et al. (2007) assimilated synthetic CryoSat sea ice thickness into a coupled ice-ocean model using an Ensemble Kalman Filter (EnKF). They found that ice thickness affected sea surface temperature, surface salinity and ice concentration and showed that ice thickness observations can have a significant impact on ice thickness estimates for the modeling system. Yang et al. (2014) utilized a Local Singular Evolutive Interpolated Kalman (LSEIK) filter in assimilating Soil Moisture Ocean Salinity (SMOS) ice thickness data into a coupled ice-ocean modeling system. In their 3-month study period beginning November 1, 2011, they found improved 24-h ice thickness forecasts with reduced biases when using this data and technique. Lindsay et al. (2012) performed seasonal forecasts of the September 2012 ice extent using ensemble predictions with the PIOMAS model initialized with a corrected ice thickness distribution based on ice thickness observations from OIB and the Seasonal Ice Zone Observation Network (SIZ-ONet). They found lower ice extent in the Pacific sector and higher extent in the Atlantic sector compared to uncorrected forecast runs.

Our study is inspired by the culmination of years of research that has led to readily-available satellite-derived ice thickness products that can be used to initialize and improve the skill in operational sea ice forecasting systems. The study by Yang et al. (2014) motivated our research by demonstrating that the assimilation of SMOS ice thickness reduced the ice thickness RMSE significantly for 24-h forecasts. Improvements such as these will not only be applicable for synoptic-scale periods, but seasonal intervals as well, such as a 4–6 month prediction of the September minimum sea ice extent. While this paper addresses the initialization of a sea ice model with satellite-derived ice

thickness, ongoing research addressing the assimilation of daily near real-time ice thickness data should yield significant advances in Arctic sea ice forecasting. The techniques addressed in this paper and the data sources used in our study should be applicable for any sea ice model.

This paper is structured as follows: Section 2 provides a background on the modeling system used in this study; Section 3 describes the techniques used to produce the ice thickness fields in this modeling study. Section 4 describes the data sources used in this study; Sections 5 presents an overview of the modeling experiments and discussion. A summary and conclusion is provided in Section 6.

2. Background

The modeling system used in this study is the Arctic Cap Nowcast/Forecast System (ACNFS) (Posey et al., 2010, 2015; Metzger et al., 2014; Hebert et al., 2015), consisting of the Los Alamos Community Ice CodE (CICE, Hunke and Lipscomb, 2008) coupled to the HYbrid Coordinate Ocean Model (HYCOM) (Chassignet et al., 2003, 2009; Metzger et al., 2014). Both CICE and HYCOM are on a the subset of a global tripole grid that is poleward of 40° N with a horizontal resolution of approximately 3.5 km at the North Pole. HYCOM has 32 vertical levels for the ocean. CICE employs five thickness categories; within each thickness category are four ice layers and one snow layer. Satellite-derived sea surface temperature, ocean and ice-tethered profiler temperature and salinity, and ice concentration data are assimilated into the ACNFS via the Navy Coupled Ocean Data Assimilation (NCODA) system (Cummings and Smedstad, 2013; Posey et al., 2015). NCODA utilizes a 3-D variational analysis (3DVAR) method to assimilate observations into the model. Ice thickness is not assimilated into the CICE model, but SSMI-based sea ice concentration is assimilated near the ice edge. HYCOM fields of sea surface temperature, sea surface salinity, and surface ocean currents are exchanged hourly with CICE using the Earth System Modeling Framework (ESMF) (Theurich et al., 2016); whereas CICE passes ice concentration, ice stress, heat flux through the ice, ice freeze/melt heat flux and net water flux to HYCOM. The ACNFS (both ocean and ice components) is run with atmospheric forcing (37 km (T359) resolution) from the NAVy Global Environmental Modeling System (NAVGEM) (Hogan et al., 2014). Precipitation in the CICE model is based on monthly climatological precipitation rates from the Global Precipitation Climatology Project (Adler et al., 2003) for the period 1979–2002. Precipitation rate is converted to a snowfall rate if the surface air temperature is at or below freezing. Drifting of snow is not incorporated into CICE. A monthly-varying climatological river database (Barron and Smedstad, 2002) is used to specify river discharge into the Arctic basin. Melt ponds are not enabled for the studies presented in this paper. The ACNFS CICE component was spun-up (without data assimilation) from a constant sea ice thick-

ness of 3 m for the period of 2005–2007 using the Navy Operational Global Atmospheric Prediction System (NOGAPS) atmospheric forcing until a steady state was reached. The model continued to run with data assimilation for the period of 2007–2013 with NOGAPS (Rosmond et al., 2002). In 2013 the model became operational and since then NAVGEM has been used to force the system. The model southern boundary is at 40°N where open ocean boundary conditions are provided by the Global Ocean Forecast System (GOFS 3.0) (Metzger et al., 2014) which has the same resolution as ACNFS. The ACNFS, developed by the Naval Research Laboratory Oceanography Division, was transitioned into operations at the Naval Oceanographic Office (NAVOCEANO) in September 2013. The modeling system is run once per day producing 7-day forecasts of both ice and ocean fields such as ice thickness, ice concentration, ice drift, sea surface temperature, sea surface salinity and ocean currents. See Hebert et al. (2015) for a more complete description of ACNFS.

3. Technique

The Ku-band (13.5 GHz) Synthetic Aperture Interferometric Radar Altimeter (SIRAL) on-board the European Space Agency's (ESA) CS2 satellite represents an advancement on previous generation satellite radar altimeters. With an instrument footprint of approximately 380 m along track by 1650 m across track, as well as the ~300 m along track sampling intervals, it represents a significant improvement over the ~10 km footprints of the heritage satellite radar altimeters and is more suitable for sea ice floe/lead discrimination and sea ice freeboard measurements (Wingham et al., 2006). Coupled with the 92° orbital inclination of CS2, SIRAL provides Arctic-wide routine observations of the sea ice freeboards and thickness up to the 88°N latitude. Three independent CS2 sea ice data processing systems have been developed by the Centre for Polar Observation and Modelling (CPOM) (Laxon et al., 2013), NASA's Goddard Space Flight Centre (GSFC) (Kurtz et al., 2014), and the Alfred Wegener Institute (AWI) (Ricker et al., 2014). The sea ice thickness data records generated by these three CS2 sea ice data systems agree reasonably well with each other in terms of spatial distribution, and provide further evidence for the long term decline of ice volume in the central Arctic. Nevertheless, significant differences exist in the estimated ice thickness among these three data sets. In addition, the summer months and the marginal ice zone are excluded from all three data sets due to snow/ice melt and open water signal contamination. Current efforts are on-going to examine different algorithm assumptions and their impacts on ice thickness retrievals (Ricker et al., 2014; Price et al., 2015; Tilling et al., 2016a, 2016b). From an ice modeling perspective, it is desirable to assimilate ice thickness data to improve sea ice prediction. On the other hand, comparisons of impacts by assimilating different ice thickness data

sets may also shed light on the retrieval algorithms themselves. To this end, we performed ice thickness reinitialization for coupled model reanalyses using the CPOM and NASA data sets. The AWI data set was not available at the time of the model runs but will be included in a future study.

3.1. Snow impacts on freeboard retrievals

CS2 freeboard is converted to ice thickness by estimating the snow load based on the Warren snow climatology (Warren et al., 1999) (W99). Utilizing snow radar data, Kurtz and Farrell (2011) found the snow cover to be approximately 50% lower than W99 on FYI ice. As a result, in processing the CS2 freeboard data, the W99 snow depths are reduced by 50% before converting the freeboard measurements to thickness of FYI ice (Laxon et al., 2013). MYI snow cover is based on the original W99 values, however some CS2 datasets apply a pan-Arctic mean climatology (Tilling et al., 2015) while others use explicit climatological values for MYI and a scale factor for FYI (Kwok and Cunningham, 2015; Ricker et al., 2014, 2015).

3.2. CPOM Arctic sea ice thickness data

Laxon et al. (2013) generated the first estimate of Arctic sea ice thickness and volume from CS2. Their algorithm first uses the CS2 Level 1B radar echo data to separate measurements of sea ice floes and leads; then determines ice floe and lead surface elevations by identifying the mean scattering horizon on the leading edge of the radar return waveform. Laxon et al. (2013) select empirically the 70% threshold of the peak power as the mean scattering horizon to track the mean surface horizon. The freeboard observations can be obtained and converted to ice thickness through equilibrium of the weight of the ice freeboard and snow to the buoyancy of the submerged ice. Since coincident snow observations are not available Arctic-wide, climatological values of snow depth and density (Warren et al., 1999) are used in the freeboard-to-thickness conversion. To extend the results of Laxon et al. (2013) outside of the central Arctic to regions where the climatology is ill-constrained by *in situ* measurements, CPOM now apply the mean snow depth and density for each month and halve the snow depth over FYI. A comprehensive validation (Tilling et al., 2015) suggests that the CS2 sea ice thickness estimates, when averaged on a large scale or over a full winter growth season, agree within 10–20 cm with independent thickness measurements from the NASA OIB (Kurtz et al., 2013), the ESA CRYOsat Validation Experiment (CryoVEx) campaign (Haas et al., 2009), and the Beaufort Gyre Exploration Project (BGEP) (Krishfield and Proshutinsky, 2006).

In this study, we use the monthly composited CPOM CS2 sea ice thickness data on 5 km square polar stereographic grid. In order to match the spatial resolution of the NASA data set, the CPOM data are projected and averaged on to a 25 km polar stereographic grid. Because the freeboard-to-thickness conversion is linear, the absolute error of ice thickness measurement does not vary with ice thickness and/or snow depth, thus the averaging is performed with equal weighting drop-in-the-bucket method. Accordingly, the ice thickness variance is reduced by a factor of the square root of the number of observations in each 25 km polar stereographic grid cell. We estimate a thickness uncertainty of ~25% for the 5 km gridded thickness (Tilling et al., 2016a, 2016b), of which the largest contributor is snow depth uncertainty (Tilling et al., 2015).

3.3. NASA Arctic sea ice thickness data

Kurtz et al. (2014) developed a CS2 physical model and waveform fitting technique (CS2WfF) that avoids the use of an empirical threshold retracker. Different from the CPOM CS2 data processing system, this NASA CS2WfF algorithm first calculates monthly mean freeboard on the 25 km polar stereographic grid, which is further smoothed to 125 km spatial resolution. Subsequently the sea ice thickness is retrieved from the 25 km CS2 freeboard data set through the hydrostatic balance based freeboard-to-thickness conversion. This algorithm is used to construct the NASA CS2WfF (Kurtz and Harbeck, 2017) Arctic sea ice thickness data. When comparing OIB airborne observations to ice thickness estimates derived from the NASA CS2WfF and a simple 50% threshold retracker, Kurtz et al. (2014) showed that the CS2WfF technique reduced their ice thickness bias. The estimated total ice thickness uncertainty is about 60 cm with contribution from a ~6 cm freeboard uncertainty. Uncertainties in snow depth are estimated at 4–6.2 cm in Warren et al. (1999), but the uncertainty contribution will scale up in the conversion of freeboard to thickness. This is also true for freeboard uncertainty.

3.4. Implementation of ice thickness fields into the model

CICE v4.0 was modified to utilize the satellite-derived ice thickness field to reinitialize the ice model. Given the model and observed total area average ice thickness: (a) if the model or observed area thickness <1 cm, no change is made; (b) otherwise we multiply each sea ice category volume (we use 5 thickness categories) by the ratio of observed over modeled sea ice thickness and directly insert the result. The same scale factor is applied to sea ice enthalpy. In this procedure, all the categories are changed by the same thickness fraction. If this pushes a category out of its range, a routine within CICE v4.0 is called to rebin the ice thickness categories.

Fig. 2 depicts the initial ice thickness fields for the modeling studies presented in this paper. Fig. 2a shows the ACNFS monthly averaged ice thickness (m) for March 2014. Fig. 2b shows the monthly averaged ice thickness field for March 2014 derived from CS2-based on the NASA algorithm (CS2-NASA, referred to as CS2WtF in previous section), while Fig. 2c depicts the monthly averaged ice
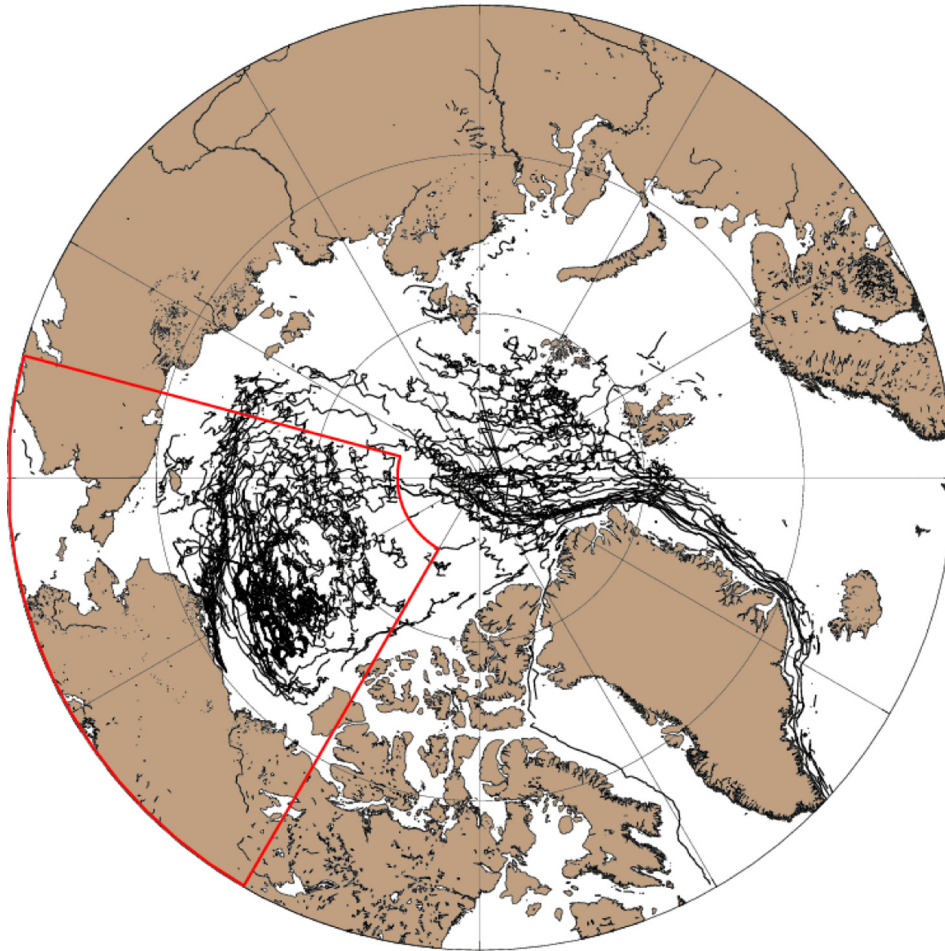
Fig. 4. Map of 288 IABP drifters for the period of March 15, 2014–September 30, 2015. Red region indicates Bering/Beaufort/Chukchi Sea domain for ice drift analysis. (For interpretation of the references to colour in this figure legend, the reader is referred to the web version of this article.)

thickness field based on the CS2 CPOM algorithm for March 2014. The March 2014 monthly averaged anomaly between CS2 and ACNFS is added to ACNFS ice thickness on March 15, 2014 for the two reanalysis studies presented in this paper. If the observed ice concentration indicates ice is present, while the CS2 ice thickness field indicates no ice is present, the data assimilation system adds 0.5 m of ice at these locations. There are noticeable differences in ice thickness along the Canadian Archipelago, and in the Bering and Beaufort Seas from the ACNFS versus the NASA and CPOM CS2-based ice thickness fields. Overall, the NASA and CPOM CS2-based fields show a thinner ice cover in the Beaufort Sea. There are also noticeable differences in the Laptev and East Siberian Seas where CS2-CPOM data set shows few ice thickness estimates.

4. Comparative data sources

4.1. Upward looking sonar

Upward Looking Sonar (ULS) ice draft data from the Woods Hole Oceanographic Institution (WHOI) BGEP

(Krishfield and Proshutinsky, 2006) for mooring locations A, B, and D (Fig. 3) are used in this study for the period of March 15, 2014–September 30, 2015. The raw data are sampled at 2 s intervals. Ice draft is converted to ice thickness by multiplying the draft by 0.89 (Rothrock et al., 2003). A daily 24-h average of the ULS data was calculated for comparisons against daily CICE model output.

4.2. Ice Mass Balance Buoys (IMBB)

"Preliminary" IMBB data from the Cold Regions Research Engineering Laboratory (CRREL) is used in our study. The buoys (Richter-Menge et al., 2006; Perovich et al., 2017) report ice thickness typically at 4-h intervals. In this study, CICE ice thickness is interpolated to daily IMBB locations at 00Z (or 03Z in limited cases) via a natural neighbor method.

4.3. NASA Operation IceBridge

NASA IceBridge "quick-look" ice thickness transects from missions flown on specific dates in March/April in 2014 are used in our study. IceBridge observations are fil-
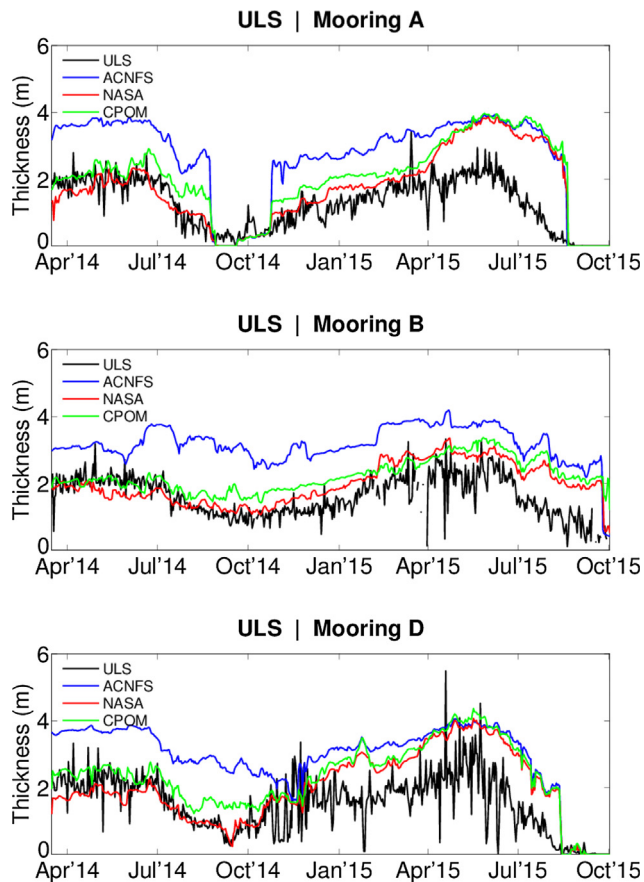
Fig. 5. Time series of modeled ice thickness (m) versus ULS moorings ice thickness observations (m) from March 15, 2014–October 2015. Black line represents observation, ACNFS is shown in blue, ACNFS reanalysis initialized with CS2-CPOM in green, and ACNFS reanalysis initialized with CS2-NASA in red. (For interpretation of the references to colour in this figure legend, the reader is referred to the web version of this article.)

tered by averaging all observations with a freeboard uncertainty less than 0.1 m within 20 km of each observation. Modeled CICE ice thickness was interpolated to the IceBridge observation locations via a natural neighbor method.

4.4. International Arctic Buoy Program (IABP)

Observed ice drift velocities are derived from daily IABP buoy locations. CICE drift components are interpolated to the IABP locations via a natural neighbor method. The IABP speed is determined by the distance the buoy traveled over 24 h. See Hebert et al. (2015) for more details on the drift calculations. In this study, 288 buoys are used. Fig. 4 depicts the drifters used in this study and the domain for the Bering/Chukchi/Beaufort Sea.

5. Discussion

5.1. Experiments

A series of reanalysis experiments are performed for the period of March 15, 2014–September 30, 2015. The

"control" experiment consisted of the ACNFS which was run operationally in real time. This control experiment, referred to as "ACNFS" did not have any adjustments made to the model's ice thickness field. Two experiments CS2-CPOM and CS2-NASA, are identical to the control run, except that the ice thickness field was corrected (one time only) on March 15, 2014 based on the CS2 (CPOM) and CS2 (NASA) monthly ice thickness anomaly fields as described in Section 3.3. In all three cases the same NAV-GEM atmospheric forcing is used and sea ice concentration and various ocean quantities are assimilated daily. In this study, we evaluate the model skill in predicting ice thickness versus ULS mooring data, IMBB, and NASA IceBridge transect data from the 2014 campaign. Fig. 3 depicts the locations of the 3 BGEP ULS stations in the Beaufort Sea and CRREL IMBB drifting in the ice during the study period. Much of this study focuses on the Bering, Chukchi, and Beaufort Seas, where a majority of the observational data was available.

5.2. ULS analysis

Ice draft data from three BGEP ULS moorings is used to evaluate the ice thickness distribution in the Navy's ACNFS model for an 18-month period beginning March 15, 2014. In this study, the CICE thickness at the grid point nearest to the daily mean observation at the ULS mooring is used in this analysis. Fig. 5 presents a time series of modeled ice thickness at the 3 ULS locations. The blue line denotes the operational ACNFS (no CS2 initialization) ice thickness at the mooring locations. The red and green lines represent experiments where the model was initialized with CS2 ice thickness anomalies from NASA and CPOM respectively. It is evident that overall, the operational ACNFS model has thicker ice throughout the 18-month period. Through October 2014, the CS2-NASA initialization experiment appears to compare best against the observational data, although the CS2-CPOM reanalysis shows lower biases through June 2014 (see Table 1). Since all 3 model simulations use identical atmospheric forcing, it is not surprising to see the ice thickness from the CS2-CPOM and NASA experiments trend toward the ACNFS ice thickness by late Spring 2015. Examination of model animations for this region showed advection of thicker ice into the Beaufort Sea, which contributed to the thicker ice beginning in October 2014, as seen at ULS station A.

Fig. 6 depicts a series of scatter plots of observed versus modeled ice thickness for all three moorings (combined) for three-month, seasonal periods beginning in April–June 2014, with summary statistics shown in the lower right of each panel. The left column represents the ACNFS experiment, middle column is CS2-CPOM, and the right column is CS2-NASA. It is evident that the ACNFS results have a positive bias throughout the 1-year period. Table 1 presents summary statistics of the combined ULS data versus the 3 ACNFS experiments. The table is divided into seasonal (3-month) periods beginning in April 1–June 30, 2014.

Table 1
Seasonal comparisons of ULS ice thickness (m) (at all locations) versus ACNFS, ACNFS simulation initialized with CS2-NASA, and ACNFS simulation initialized with CS2-CPOM. Last rows represent averages over the 18-month period. Grey boxes in columns on right indicate best performance.

Apr 1 – Jun 30, 2014	ULS	ACNFS	NASA	CPOM
Mean (m)	2.07	3.52	1.84	2.27
Bias		1.44	-0.23	0.20
RMSE		1.52	0.44	0.44
R^2		-0.09	-0.04	0.09
Jul 1 – Sep 30, 2014				
Mean (m)	1.02	2.58	1.02	1.50
Bias		1.56	-0.01	0.47
RMSE		1.74	0.28	0.61
R^2		0.72	0.84	0.77
Oct 1– Dec 31, 2014				
Mean (m)	1.13	2.43	1.41	1.70
Bias		1.29	0.28	0.57
RMSE		1.48	0.56	0.77
R^2		0.38	0.56	0.51
Jan 1– Mar 31, 2015				
Mean (m)	1.72	3.29	2.39	2.53
Bias		1.55	0.66	0.80
RMSE		1.60	0.83	0.95
R^2		0.42	0.33	0.19
Apr 1, 2014-Sep 30, 2015				
Mean (m)	1.45	2.89	1.92	2.20
Bias		1.44	0.47	0.75
RMSE		1.60	0.89	1.04
R^2		0.74	0.64	0.66

For this first season, both the CPOM and NASA experiments show low biases of near ±20 cm with a RMSE of 0.44 m. Surprisingly, all three experiments show poor correlation for this period. We attribute this to modulations in the observed ice thickness which are not captured well by the model. The summer period of July 1–September 30, 2014 shows that the mean ice thickness from the CS2-NASA reanalysis had the identical mean thickness compared to the ULS means, with the smallest bias (−0.01) and RMSE (0.28) and highest correlation at 0.84. The CS2-CPOM reanalysis showed thicker ice than CS2-NASA, but demonstrated a noticeable improvement over the ACNFS operational results. The autumn period from October 1–December 31, 2014 shows that the CS2-NASA reanalysis outperforms ACNFS and CS2-CPOM. By the winter period of January 1–March 31, 2015, the bias and RMSE for both CS2 reanalysis studies continue to increase. While the ACNFS results show a better correlation coefficient (0.42), the CS2- NASA and CPOM reanalyses continue to outperform the ACNFS in terms of ice thickness, bias and RMSE. The last section in the table shows the mean statistics for the entire 18-month period.

Overall, the reanalysis initialized with CS2-NASA showed the lowest bias (0.47) and RMSE (0.89), although it also exhibited the lowest correlation (0.64).

5.3. IMBB results

Fig. 7 depicts model/data comparisons against 3 CRREL IMBB deployed in the Beaufort Sea during this study period (Fig. 3). All three buoys generally drift toward the west-northwest, except for 2013F which has a mean drift toward the northwest. The operational ACNFS ice thickness is approximately 1.5 m too thick for much of the study period. The CS2-NASA and CS2-CPOM reanalyses show much better agreement to observations at 2013F for the period of March 2014 through late October, 2014. Afterwards, the modeled ice thickness begins to get thicker compared to observation. At 2014B and 2014C, the CS2-NASA reanalysis shows a remarkable agreement to the observations through June 2014. Afterwards, the CS2-CPOM reanalysis more closely matches the observed ice thickness. Table 2 summarizes these results for the entire model/data comparison period. Overall, CS2-NASA shows
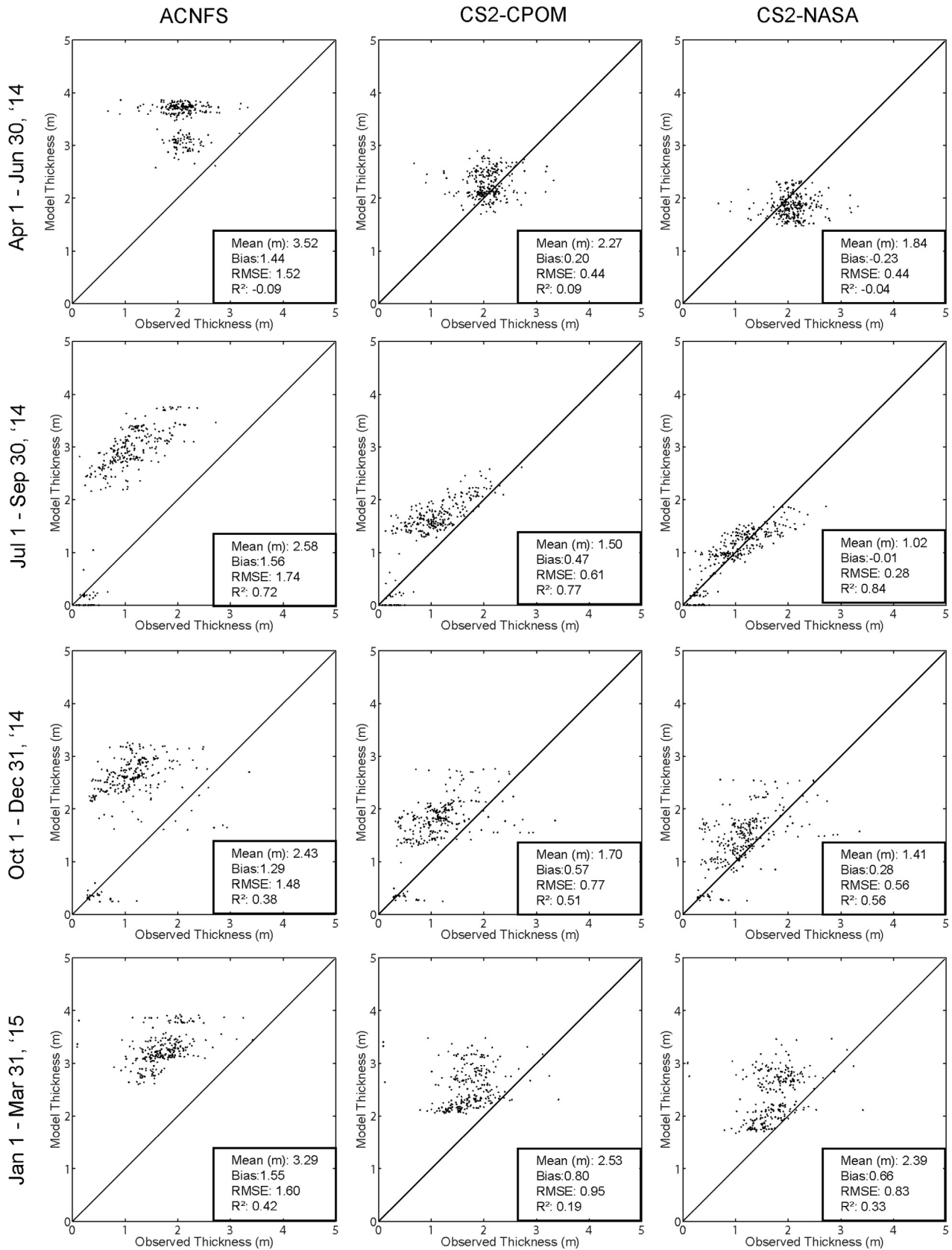
Fig. 6. Scatter plots of observed versus model ice thickness (m) at ULS moorings ice thickness observations in seasonal groupings. Top row represents Spring 2014 (April–June), followed by Summer 2014 (July–September), Autumn 2014 (October–December), and Winter 2015 (January–March). Column on left represents ACNFS simulations, followed by ACNFS reanalysis initialized with CS2-CPOM (middle), and ACNFS reanalysis initialized with CS2-NASA (right).
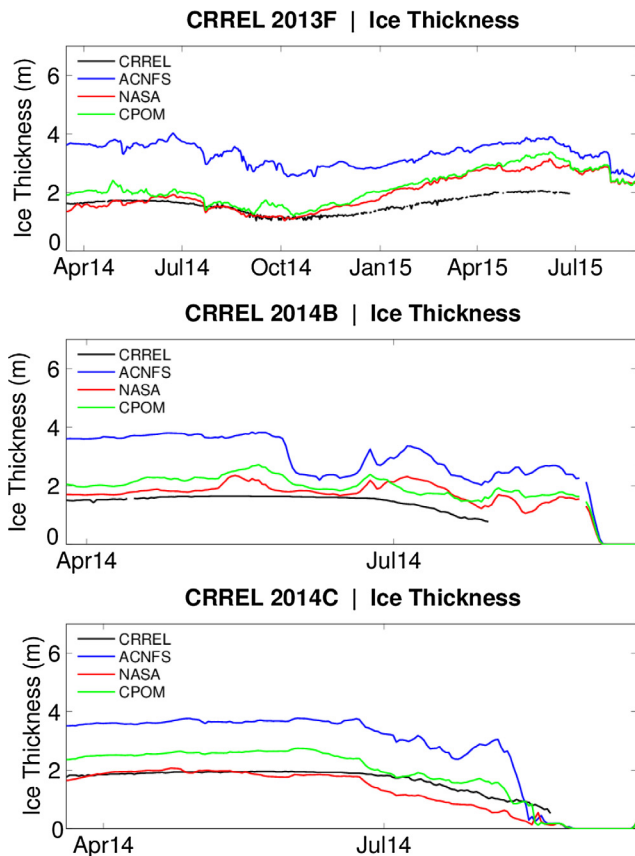
Fig. 7. Time series of modeled ice thickness (m) versus observed CRREL Ice Mass Balance Buoy thickness for inclusive periods of March 15, 2014–Sept 2015. Blue line represents ACNFS, green line denotes ACNFS reanalysis initialized with CS2-CPOM, and red line represents ACNFS Reanalysis initialized with CS2-NASA. (For interpretation of the references to colour in this figure legend, the reader is referred to the web version of this article.)

the best agreement to with the observations for mean thickness, lowest bias and RMSE. The CS2-CPOM reanalysis showed the highest correlation (tie at 2014C in R^2). We also looked at a Central Arctic IMBB 2015D (not shown), and it showed very similar results between all three model studies presented in this paper. This IMBB was deployed in April 2015, about 1 year after our study began. The model/data comparisons showed excellent agreement with observations until July 2015, when the modeled ice thickness began to get thicker versus the observed ice thickness. This provided some insight suggesting that the CS2 ice thickness product (from either CPOM or NASA) was realistic for the Central Arctic at the beginning of our study period.

5.4. NASA IceBridge results

To further assess the accuracy of the CS2 ice thickness products from both NASA and CPOM, we compared the modeled ice thickness in this study against NASA OIB data collected in March and April 2014. Fig. 8 depicts the eight IceBridge transects used in our study. Fig. 9 depicts a scat-

ter plot of observed ice thickness from NASA's quick-look data set versus model results from ACNFS, CS2-CPOM, and CS2-NASA. Both the CS2- NASA and CPOM results show a better comparison with modeled ice thickness. Table 3 presents statistics for these comparisons. The CS2-NASA reanalysis study showed the closest match to the mean calculated for these transects (2.61 versus 2.57 m), with a lower bias at −0.01 m. The RMSE and correlation coefficients for both CS2 reanalyses are very similar.

5.5. IABP results

We examined ice drift for the full Pan-Arctic from the ACNFS (operational, CS2-CPOM, and CS2-NASA) simulations versus ice drift calculated from the 288 IABP buoys (Fig. 4) for the period of March 15, 2014–September 30, 2015. Over 44,000 ice drift observations were examined in this analysis. Overall, the ACNFS ice drift magnitude (not shown) was in better agreement with observations with an error of 9.9% versus errors of 11.9% (CS2-CPOM) and 12.9% (CS2-NASA). The CS2 experiments are within approximately 1.2–1.3 cm/s in magnitude of the calculated IABP drift over the 18-month period. We further investigated the ice drift in the Bering/Chukchi/Beaufort Seas for this same period. Table 4 presents a summary of the analysis in which this subset of 26,806 IABP observations were examined. Similar to the Pan-Arctic region, the CS2 experiments exhibit faster ice drift than ACNFS and observations. Since the ice is overall thinner and wind speeds are the same as the operational ACNFS runs, one expects to see the faster drifts. We also examined the drift during the summer/autumn months in 2014 and it showed that the CS2-NASA and CS2-CPOM experiments exhibited a 29% and 24% reduction in ice drift magnitude error, respectively, compared to ACNFS (see Table 5). We also see improvement during the period of July–September, 2015 as well, but to a lesser extent. Summertime improvements are also evident in the Greenland/Norwegian Seas (not shown).

6. Conclusion and plans

Previous studies (Holland et al. 2011; Day et al., 2014) showed the importance of sea ice model initialization with ice thickness fields in predicting the ensuing summer minimum ice extent. In this study, the U.S. Navy's coupled sea-ice modeling system ACNFS is initialized with monthly sea ice thickness fields obtained from two different CS2 data sources which are derived using differing techniques. The CS2-CPOM dataset is based on an empirical leading-edge 70% threshold retracker and is interpolated from a 5 km square polar stereographic grid and averaged onto a 25 km polar stereographic grid for this study. The CS2-NASA dataset is based on a threshold retracking algorithm and is gridded on a 25 km stereographic grid.

Our results are in good agreement with the ice thickness RMSE shown by Yang et al. (2014) where they

Table 2
Summary statistics for CRREL Ice Mass Balance Buoy ice thickness (m) versus ACNFS, ACNFS simulation initialized with CS2-NASA, and ACNFS simulation initialized with CS2-CPOM. Grey boxes in columns on right indicate best performance.

		ACNFS	**NASA**	**CPOM**
	2013F			
Mean (m)	1.58	3.34	1.89	2.12
Bias		1.76	0.31	0.54
RMSE		1.77	0.48	0.64
R^2		0.85	0.85	0.89
	2013B			
Mean (m)	1.49	3.18	1.86	2.07
Bias		1.69	0.38	0.58
RMSE		1.77	0.45	0.61
R^2		0.54	0.40	0.78
	2014C			
Mean (m)	1.69	3.19	1.48	2.14
Bias		1.50	-0.21	0.45
RMSE		1.59	0.33	0.55
R^2		0.90	0.94	0.94

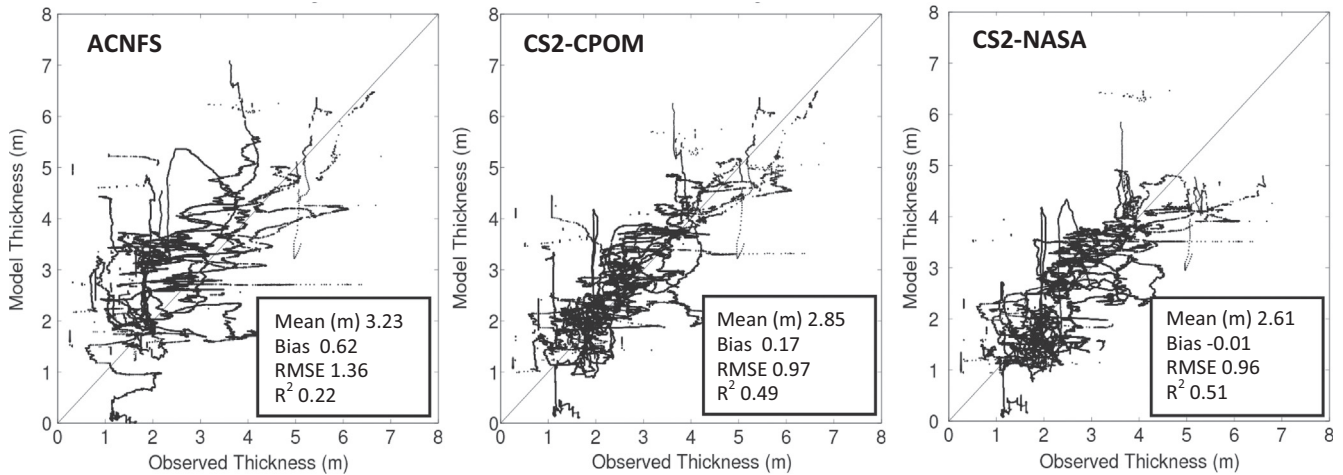Fig. 8. NASA Operation IceBridge tracks used in analysis versus modeled ice thickness for March/April 2014.

Fig. 9. Scatter plots of observed NASA IceBridge (2014) ice thickness (m) versus ice thickness from ACNFS (left), ACNFS CS2-CPOM initialized simulations (middle), and ACNFS initialized with CS2-NASA (right).

Table 3
Summary statistics for NASA IceBridge (March/April 2014) thickness (m) versus ACNFS, ACNFS simulation initialized with NASA-CS2, and ACNFS simulation initialized with CS2-CPOM. Grey boxes in columns on right indicate best performance.

	IceBridge Average	ACNFS	NASA	CPOM
Mean (m)	2.57	3.23	2.61	2.85
Bias		0.62	-0.01	0.17
RMSE		1.36	0.96	0.97
R^2		0.22	0.51	0.49

Table 4
Mean ice drift statistics for the Bering/Chukchi/Beaufort Sea for the period of March 15, 2014–September 30, 2015. Comparisons consist of observed ice drift from IABP-derived ice drift versus modeled ice drift. Greyed boxes indicate smallest error against observations.

Bering/Chukchi /Beaufort	Observed (26805)	ACNFS	NASA	CPOM
Magnitude (cm/s)	10.1	10.2	10.7	10.6
U-Comp (cm/s)	7.2	7.2	7.6	7.5
V-Comp (cm/s)	5.5	5.8	5.9	5.9

assimilated SMOS ice thickness in the MITgcm model for a 3-month period from November 2011–January 2012. Our study shows that the model's ice thickness is significantly improved compared against observed moored, drifting and airborne measurements using both the NASA and CPOM CS2 initialization versus the oper-

ational ACNFS which is not initialized with these data sources. In addition, the modeling system initialized with both CS2 data sets exhibits skill up to the first 6 months when compared against ULS and IMBB data. In particular, based on the data periods examined here, the CS2-NASA reanalysis shows a vastly improved average ice

Table 5
Monthly-averaged Ice drift magnitude (cm/s) for the Bering/Chukchi/Beaufort Sea from IABP-derived ice drift versus modeled ice drift for June–November, 2014. Greyed boxes indicate closest agreement to observations.

Bering/Chukchi/Beaufort Sea	# of Obs	Observed Mag. (cm/s)	ACNFS Mag. (cm/s)	NASA Mag. (cm/s)	CPOM Mag. (cm/s)
Jun 2014	2263	12.1	9.9	10.6	10.5
Jul 2014	2385	11.1	10.2	10.7	10.6
Aug 2014	2144	13.3	11.2	11.8	11.8
Sep 2014	1494	14.9	12.8	13.5	13.4
Oct 2014	1460	14.7	12.5	12.6	12.6
Nov 2014	940	11.8	11.2	11.4	11.3
% Improvement over ACNFS			---	29	24

thickness bias (versus ACNFS) to less than 50 cm for the full 18-month period when comparing against all the moored and drifting data. The CS2-CPOM data is provided on a 5 km grid and here we interpolated onto a 25 km grid for consistency with the CS2-NASA data, although the spatial resolution of the NASA data is effectively 125 km due to smoothing. We did not perform experiments with the 5 km CPOM ice thickness data or smooth the 25 km gridded CS2-CPOM data, so we are unable to comment on the impact of a different spatial resolutions on the model results.

An analysis of ice drift data from the IABP shows that for the Pan-Arctic and Bering/Beaufort/Chukchi (BBC) regions, the operational ACNFS modeling system slightly outperformed the CS2-initialized experiments. However, we see an improvement during the summer/autumn period in 2014 in the BBC region where the ice drift magnitude from both the CS2-NASA and CS2-CPOM initialization outperformed the operational model.

This paper addresses the initialization of a sea ice model using CS2 data from two different sources. Ongoing research is investigating the assimilation of daily ice thickness data from altimeters onboard CS2 and Sentinel-3A. Modelers will need to examine tradeoffs between utilizing near-realtime data provided by sources such as CS2-CPOM versus ice thickness products from providers such as CS2-NASA (hosted by NSIDC) which has a latency of ~1 month. Future plans include investigating the reinitialization of our modeling system using an autumn (October or November) period in which the ice is thinner than the March initialization period studied here. The same data sources discussed in this paper (CS2-NASA and CS2-CPOM) will be used. We also plan to test a merged CS2/SMOS ice thickness product, since CS2 is more accurate for ice greater than approximately 0.5 m thickness while SMOS is more appropriate for thinner ice. Lastly, we also plan to perform tests with the anticipated ICESat-2 ice

thickness fields, which could also be used to reinitialize the Navy's ice modeling systems.

References

Adler, R.F., Huffman, G.J., Chang, A., Ferraro, R., Xie, P., Janowiak, J., Rudolf, B., Schneider, U., Curtis, S., Bolvin, D., Gruber, A., Susskind,

J., Arkin, P., Nelkin, E., 2003. The version-2 Global Precipitation Climatology Project (GPCP) monthly precipitation analysis (1979-Present). J. Hydrometeor. 4, 1147–1167.

Barron, C.N., Smedstad, L.F., 2002. Global river inflow within the Navy Coastal Ocean Model. In: OCEANS '02 MTS/IEEE, vol. 3, pp. 1472–1479. 10.1109/OCEANS.2002.1191855.

Blanchard-Wrigglesworth, E., Bitz, C.M., 2014. Characteristics of Arctic sea-ice thickness variability in GCMs. J. Clim. 27 (21), 8244–8258.

Chassignet, E.P., Smith, L.T., Halliwell, G.R., Bleck, R., 2003. North Atlantic simulations with the HYbrid Coordinate Ocean Model (HYCOM): impact of the vertical coordinate choice, reference pressure, and thermobaricity. J. Phys. Oceanogr. 33, 2504–2526. https://doi.org/10.1175/1520-0485(2003) 033.

Chassignet, E.P., Hurlburt, H.E., Metzger, E.J., Smedstad, O.M., Cummings, J.A., Halliwell, G.R., Bleck, R., Baraille, R., Wallcraft, A.J., Lozano, C., et al., 2009. US GODAE: global ocean prediction with the HYbrid Coordinate Ocean Model (HYCOM). Oceanography 22 (2), 64–75. https://doi.org/10.5670/oceanog.2009.39.

Collow, T.W., Wang, W., Kumar, A., Zhang, J., 2015. Improving Arctic sea ice prediction using PIOMAS initial sea ice thickness in a coupled ocean–atmosphere model. Mon. Weather Rev. 143 (11), 4618–4630.

Cummings, J.A., Smedstad, O.M., 2013. Variational data assimilation for the global ocean. In: Park, S.K., Xu, L. (Eds.), Data Assimilation for Atmospheric, Oceanic and Hydrologic Applications. Springer-Verlag, Berlin Heidelberg, pp. 303–343. https://doi.org/10.1007/978-3-642-35088-7_1310.1007/978-3-642- 35088-7_13.

Day, J.J., Hawkins, E., Tietsche, S., 2014. Will Arctic sea ice thickness initialization improve seasonal forecast skill? Geophys. Res. Lett. 41 (21), 7566–7575.

Farrell, S.L., Kurtz, N., Connor, L., Elder, B., Leuschen, C., Markus, T., McAdoo, D.C., Panzer, B., Richter-Menge, J., Sonntag, J., 2012. A first assessment of IceBridge snow and ice thickness data over Arctic sea ice. IEEE Trans. Geosci. Remote Sens. 50 (6). https://doi.org/10.1109/TGRS.2011.2170843.

Giles, K.A., Laxon, S.W., Wingham, D.J., Wallis, D.W., Krabill, W.B., Leuschen, C.J., McAdoo, D., Manizade, S.S., Raney, R.K., 2007. Combined airborne laser and radar altimeter measurements over the Fram Strait in May 2002. Remote Sens. Environ. 111 (2), 182–194.

Guemas, V., Blanchard-Wrigglesworth, E., Chevallier, M., Day, J.J., Déqué, M., Doblas-Reyes, F.J., Fučkar, N.S., Germe, A., Hawkins, E., Keeley, S., Koenigk, T., 2016. A review on Arctic sea-ice predictability and prediction on seasonal to decadal time-scales. Q. J. R. Meteorolog. Soc. 142 (695), 546–561.

Haas, C., Pfaffling, A., Hendricks, S., Raberstein, L., Etienne, J.-L., Rigor, I., 2008. Reduced ice thickness in Arctic Transpolar Drift favors rapid ice retreat. Geophys. Res. Lett. 35, L17701. https://doi.org/10.1029/2008GL034457.

Haas, C., Lobach, J., Hendricks, S., Rabenstein, L., Pfaffling, A., 2009. Helicopter-borne measurements of sea ice thickness, using a small and lightweight, digital EM system. J. Appl. Geophys. 67 (3), 234–241. https://doi.org/10.1016/j.jappgeo.2008.05.005.

Haas, C., Hendricks, S., Eicken, H., Herber, A., 2010. Synoptic airborne thickness surveys reveal state of Arctic sea ice cover. Geophys. Res. Lett. 37, L09501. https://doi.org/10.1029/2010GL042652.

Hebert, D.A., Allard, R.A., Metzger, E.J., Posey, P.G., Preller, R.H., Wallcraft, A.J., Phelps, M.W., Smedstad, O.M., 2015. Short-term sea ice forecasting: an assessment of ice concentration and ice drift forecasts using the U.S. Navy's Arctic Cap Nowcast/Forecast System. J. Geophys. Res. Oceans 120, 8327–8345. https://doi.org/10.1002/2015JC011283.

Hogan, T.F., Liu, M., Ridout, J.A., Peng, M.S., Whitcomb, T.R., Ruston, B.C., Reynolds, C.A., Eckermann, S.D., Moskaitis, J.R., Baker, N.L., McCormack, J.P., Viner, K.C., McLay, J.G., Flatau, M.K., Xu, L., Chen, C., Chang, S.W., 2014. The navy global environmental model. Oceanography 27 (3), 116–125. https://doi.org/10.5670/oceanog.2014.73.

Holland, M.M., Bailey, D.A., Vavrus, S., 2011. Inherent sea ice predictability in the rapidly changing Arctic environment of the Community Climate System Model, version 3. Clim. Dyn. 36 (7–8), 1239–1253.

Hunke, E., Lipscomb, W., 2008. CICE: The Los Alamos Sea Ice Model Documentation and Software User's Manual Version 4.0. Tech. Rep. LA-CC-06-012. Los Alamos Natl. Lab., Los Alamos, NM.

Johnson, M., Proshutinsky, A., Aksenov, Y., Nguyen, A.T., Lindsay, R., Haas, C., Zhang, J., Diansky, N., Kwok, R., Maslowski, W., Häakkinen, S., Ashik, I., de Cuevas, B., 2012. Evaluation of Arctic sea ice thickness simulated by Arctic Ocean Model Intercomparison Project models. J. Geophys. Res. 117, C00D13. https://doi.org/10.1029/2011JC007257.

King, J., Howell, S., Derksen, C., Rutter, N., Toose, P., Beckers, J.F., Haas, C., Kurtz, N., Richter-Menge, J., 2015. Evaluation of operation IceBridge quick-look snow depth estimates on sea ice. Geophys. Res. Lett. 42, 9302–9310. https://doi.org/10.1002/2015GL066389.

Krishfield, R., Proshutinsky, A., 2006. BGOS ULS Data Processing Procedure. Woods Hole Oceanographic Institution, March 2006, 14 pp.

Kurtz, N.T., Farrell, S.L., 2011. Large-scale surveys of snow depth on Arctic sea ice from Operation IceBridge. Geophys. Res. Lett. 38, L20505. https://doi.org/10.1029/2011GL049216.

Kurtz, N.T., Farrell, S.L., Studinger, M., Galin, N., Harbeck, J.P., Lindsey, R., Onana, V.D., Panzer, B., Sonntag, J.G., 2013. Sea ice thickness, freeboard, and snow depth products from Operation IceBridge airborne data. Cryosphere 7, 1035–1056. https://doi.org/10.5194/tc-7/1035-2013.

Kurtz, N.T., Galin, N., Studinger, M., 2014. An improved CryoSat-2 sea ice freeboard retrieval algorithm through the use of waveform fitting. Cryosphere 8, 1217–1237. https://doi.org/10.5194/tc-8-1217-2014.

Kurtz, N., Harbeck, J., 2017. CryoSat-2 Level 4 Sea Ice Elevation, Freeboard and Thickness. Version 1. Boulder, Colorado USA. NASA National Snow and Ice Data Center Distributed Active Archive Center.

Kwok, R., Cunningham, G.F., 2015. Variability of Arctic sea ice thickness and volume from CryoSat-2. Philos. Trans. Roy. Soc. A-Math. Phys. Eng. Sci. 373, 20140157.

Kwok, R., Cunningham, G.F., Zwally, H.J., Yi, D., 2007. Ice, Cloud, and land Elevation Satellite (ICESat) over Arctic sea ice: retrieval of freeboard. J. Geophys. Res. 112, C12013. https://doi.org/10.1029/2006JC003978.

Kwok, R., Cunningham, G.F., Wensnahan, M., Rigor, I., Zwally, H.J., Yi, D., 2009. Thinning and volume loss of the Arctic Ocean sea ice cover: 2003–2008. J. Geophys. Res. 114, C07005. https://doi.org/10.1029/2009JC005312.

Kwok, R., Rothrock, D.A., 2009. Decline in Arctic sea ice thickness from submarine and ICESat records: 1958–2008. Geophys. Res. Lett. 36, L15505. https://doi.org/10.1029/2009GL039035.

Laxon, S., Peacock, N., Smith, D., 2003. High interannual variability of sea ice thickness in the Arctic region. Nature 425, 947–950.

Laxon, S.W., Giles, K.A., Ridout, A.L., Wingham, D.J., Willatt, R., Cullen, R., Kwok, R., Schweiger, A., Zhang, J., Haas, C., Hendricks, S., Krishfield, R., Kurtz, N., Farrell, S., Davidson, M., 2013. CryoSat-2 estimates of Arctic sea ice thickness and volume. Geophys. Res. Lett. 40, 732–737. https://doi.org/10.1002/grl.50193.

Lindsay, R.W., Zhang, J., Schweiger, A.J., Steele, M.A., 2008. Seasonal predictions of ice extent in the Arctic Ocean. J. Geophys. Res. Oceans 113 (C2).

Lindsay, R., Haas, C., Hendricks, S., Hunkeler, P., Kurtz, N., Paden, J., Panzer, B., Sonntag, J., Yungel, J., Zhang, J., 2012. Seasonal forecasts of Arctic sea ice initialized with observations of ice thickness. Geophys. Res. Lett. 39, L21502. https://doi.org/10.1029/2012GL053576.

Lisæter, K.A., Evensen, G., Laxon, S., 2007. Assimilating synthetic CryoSat sea ice thickness in a coupled ice-ocean model. J. Geophys. Res. 112, C07023. https://doi.org/10.1029/2006JC003786.

Markus, T., Stroeve, J.C., Miller, J., 2009. Recent changes in Arctic sea ice melt onset, freezeup, and melt season length. J. Geophys. Res. 114, C12024. https://doi.org/10.1029/2009JC005436.

Metzger, E.J., Smedstad, O.M., Thoppil, P.G., Hurlburt, H.E., Cummings, J.A., Wallcraft, A.J., Zamudio, L., Franklin, D.S., Posey, P.G., Phelps, M.W., Hogan, P.J., Bub, F.L., DeHaan, C.J., 2014. US Navy operational global ocean and Arctic ice prediction systems. Oceanography 27 (3), 32–43. https://doi.org/10.5670/oceanog.2014.66.

Parkinson, C.L., Cavalieri, D.J., 2008. Arctic sea ice variability and trends, 1979–2006. J. Geophys. Res. 113, C07003. https://doi.org/10.1029/2007JC004558.

Perovich, D., Richter-Menge, J., Elder, B., Arbetter, T., Claffey, K., Polashenski, C., 2017. Observing and understanding climate change: monitoring the mass balance, motion, and thickness of Arctic sea ice. <http://imb.erdc.dren.mil>.

Perovich, D., Meier, W., Tschudi, M., Farrell, S., Gerland, S., Hendricks, S., Krumpen, T., Haas, C., 2016. Sea Ice (in Arctic Report Card 2016). <http://www.arctic.noaa.gov/reportcard>.

Posey, P.G., Metzger, E.J., Wallcraft, A.J., Preller, R.H., Smedstad, O.M., Phelps, M.W., 2010. Validation of the 1/128 Arctic Cap Nowcast/Forecast System (ACNFS). Tech. Rep. NRL/MR/7320-10-9287. Naval Res. Lab., Stennis Space Center, MS.

Posey, P.G., Metzger, E.J., Wallcraft, A.J., Hebert, D.A., Allard, R.A., Smedstad, O.M., Phelps, M.W., Fetterer, F., Stewart, J.S., Meier, W. N., Helfrich, S.R., 2015. Assimilating high horizontal resolution sea ice concentration data into the US Navy's ice forecast systems: arctic Cap Nowcast/Forecast System (ACNFS) and the Global Ocean Forecast System (GOFS 3.1). Cryosphere 9, 2339–2365. https://doi.org/10.5194/tcd-9-2339-2015.

Price, D., Beckers, J., Ricker, R., Kurtz, N., Rack, W., Haas, C., Helm, V., Hendricks, S., Leonard, G., Langhorne, P.J., 2015. Evaluation of CryoSat-2 derived sea-ice freeboard over fast ice in McMurdo Sound, Antarctica. J. Glaciol. 61 (226). https://doi.org/10.3189/2015JoG14J157.

Richter-Menge, J.A., Perovich, D.K., Elder, B.C., Claffey, K., Rigor, I., Ortmeyer, M., 2006. Ice mass balance buoys: a tool for measuring and attributing changes in the thickness of the Arctic sea ice cover. Ann. Glaciol. 44, 205–210.

Richter-Menge, J.A., Farrell, S.L., 2013. Arctic sea ice conditions in spring 2009–2013 prior to melt. Geophys. Res. Lett. 40, 5888–5893. https://doi.org/10.1002/2013GL058011.

Ricker, R., Hendricks, S., Helm, V., Skourup, H., Davidson, M., 2014. Sensitivity of CryoSat-2 Arctic sea-ice freeboard and thickness on radar-waveform interpretation. Cryosphere 8 (4), 1607–1622.

Ricker, R., Hendricks, S., Perovich, D.K., Helm, V., Gerdes, R., 2015. Impact of snow accumulation on CryoSat-2 range retrievals over Arctic sea ice: an observational approach with buoy data. Geophys. Res. Lett. 42, 4447–4455. https://doi.org/10.1002/2015GL064081.

Rosmond, T.E., Teixeira, J., Peng, M., Hogan, T.F., Pauley, R., 2002. Navy Operational Global Atmospheric Prediction System (NOGAPS): forcing for ocean models. Oceanography 15 (1), 99–108. https://doi.org/10.5670/oceanog.2002.40.

Rothrock, D.A., Zhang, J., Yu, Y., 2003. The Arctic ice thickness anomaly of the 1990s: a consistent view from observations and models. J. Geophys. Res. 108, 3083. https://doi.org/10.1029/2001JC001208.

Schweiger, A., Lindsay, R., Zhang, J., Steele, M., Stern, H., Kwok, R., 2011. Uncertainty in modeled Arctic sea ice volume. J. Geophys. Res. 116, C00D06. https://doi.org/10.1029/2011JC007084.

Theurich, G., DeLuca, C., Campbell, T., Liu, F., Saint, K., Vertenstein, M., Chen, J., Oehmke, R., Doyle, J., Whitcomb, T., Wallcraft, A., Irdell, M., Black, T., Da Silva, A.M., Clune, T., Ferraro, R., Li, P., Kelley, M., Aleinov, I., Balaji, V., Zadeh, N., Jacob, R., Kirtman, B., Giraldo, F., McCarren, D., Sandgathe, S., Peckham, S., Dunlap IV, R., 2016. The Earth System Prediction Suite: toward a coordinated U. S. modeling capability. Bull. Am. Meteor. Soc. 97, 1229–1247. https://doi.org/10.1175/BAMS-D-14-00164.1.

Tilling, R., Ridout, A., Shepherd, A., Wingham, D., 2015. Increased Arctic sea ice volume after anomalously low melting in 2013. Nat. Geosci. 8, 643–648. https://doi.org/10.1038/NGEO2489.

Tilling, R., Ridout, A., Shepherd, A., 2016a. A comparison of four estimates of Arctic sea ice thickness and volume. In: AGU Fall Meeting, San Francisco, CA.

Tilling, R.L., Ridout, A., Shepherd, A., 2016b. Near-real-time Arctic sea ice thickness and volume from CryoSat-2. Cryosphere 10, 2003–2012. https://doi.org/10.5194/tc-10-2003-2016.

Tschudi, M.A., Stroeve, J.C., Stewart, J.S., 2016. Relating the age of Arctic sea ice to its thickness, as measured during NASA's ICESat and IceBridge Campaigns. Remote Sens. 8, 457. https://doi.org/10.3390/rs8060457.

Yang, Q., Losa, S.N., Losch, M., Tian-Kunze, X., Nerger, L., Liu, J., Kaleschke, L., Zhang, Z., 2014. Assimilating SMOS sea ice thickness into a coupled ice-ocean model using a local SEIK filter. J. Geophys. Res. Oceans 119, 6680–6692. https://doi.org/10.1002/2014JC009963.

Warren, S.G., Rigor, I.G., Untersteiner, N., Radionov, V.F., Bryazgin, N. N., Aleksandrov, Y.I., Colony, R., 1999. Snow depth on Arctic sea ice. J. Clim. 12 (6), 1814–1829.

Webster, M.A., Rigor, I.G., Nghiem, S.V., Kurtz, N.T., Farrell, S.L., Perovich, D.K., Sturm, M., 2014. Interdecadal changes in snow depth on Arctic sea ice. J. Geophys. Res. Oceans 119, 5395–5406. https://doi.org/10.1002/2014JC009985.

Wingham, D.J., Francis, C.R., Baker, S., et al., 2006. CryoSat: a mission to determine the fluctuations in Earth's land and marine ice fields. Adv. Space Res. 37 (4), 841–871.